Princeton Plasma Physics Laboratory

PPPL- 4310

PPPL- 4310

Plasma-Sheath Instability in Hall Thrusters Due to Periodic Modulation of the Energy of Secondary Electrons in Cyclotron Motion

D. Sydorenko and A. Smolyakov I. Kaganovich and Y. Raitse

April 2008

Prepared for the U.S. Department of Energy under Contract DE-AC02-76CH03073.

Princeton Plasma Physics Laboratory
Report Disclaimers

Full Legal Disclaimer

Trademark Disclaimer

PPPL Report Availability

Princeton Plasma Physics Laboratory:

http://www.pppl.gov/techreports.cfm

Office of Scientific and Technical Information (OSTI):

http://www.osti.gov/bridge

Related Links:

U.S. Department of Energy

Office of Scientific and Technical Information

Fusion Links

Plasma-sheath instability in Hall thrusters due to periodic modulation of the energy of secondary electrons in cyclotron motion

D. Sydorenko* and A. Smolyakov
Department of Physics and Engineering Physics, University of Saskatchewan, Saskatoon, Saskatchewan S7N 5E2, Canada

I. Kaganovich and Y. Raitses
Princeton Plasma Physics Laboratory, Princeton University, Princeton, New Jersey 08543, USA

Particle-in-cell simulation of Hall thruster plasmas reveals a plasma-sheath instability manifesting itself as a rearrangement of the plasma sheath near the thruster channel walls accompanied by a sudden change of many discharge parameters. The instability develops when the sheath current as a function of the sheath voltage is in the negative conductivity regime. The major part of the sheath current is produced by beams of secondary electrons counter-streaming between the walls. The negative conductivity is the result of nonlinear dependence of beam-induced secondary electron emission on the plasma potential. The intensity of such emission is defined by the beam energy. The energy of the beam in crossed axial electric and radial magnetic fields is a quasi-periodical function of the phase of cyclotron rotation, which depends on the radial profile of the potential and the thruster channel width. There is a discrete set of stability intervals determined by the final phase of the cyclotron rotation of secondary electrons. As a result, a small variation of the thruster channel width may result in abrupt changes of plasma parameters if the plasma state jumps from one stability interval to another.

PACS numbers: 52.35.Mw, 52.40.Kh, 52.65.Rr

I. INTRODUCTION

Hall thrusters (HT) are discharge devices for spacecraft propulsion.[1] A typical HT has a ceramic coaxial channel in which many important processes occur. Ions are accelerated by an intense axial electric field near the exit plane of the thruster, in the so-called acceleration region, where the electron mobility along the thruster axis is suppressed by a strong radial magnetic field. In a wide range of HT parameters, a part of the acceleration region with strong electric field and high electron temperature is located inside the thruster channel.[2] The neutral gas pressure in the acceleration region is extremely low and the electron mean free path greatly exceeds the width of the channel. In this kinetic collisionless regime, the electron velocity distribution function (EVDF) becomes highly unusual as compared to a common glow discharge, where the electron mean free path is smaller than a typical discharge dimension.[3]

Kinetic properties of HT plasmas are addressed, for example, in Refs. 4–8. Recently, a number of kinetic studies of plasmas in the acceleration region of a Hall thruster have been carried out by the authors using particle-in-cell (PIC) simulations.[9–12] The model developed by the authors considers a plasma slab bounded by dielectric walls with secondary electron emission (SEE) and immersed in the constant electric field E_z directed parallel to the walls and magnetic field B_x directed normal to the walls, as shown in Fig. 1. Such a configuration is very close to that of the so-called linear Hall thrusters.[13,14] The model is implemented in the form of a 1D3V PIC code. A detailed description of the PIC code is given in Ref. 15. All simulations described below are carried out with this code.

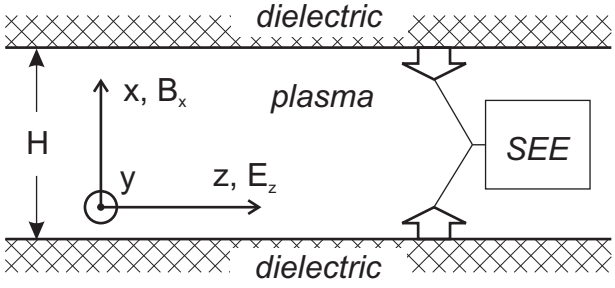

FIG. 1: Schematic diagram of the Hall thruster model. The two dielectric walls represent the coaxial ceramic channel of a Hall thruster.

It was found that the EVDF can be very anisotropic, with the electron temperature in one direction much larger than in the other direction.[9] The high-energy tails of the EVDF can be depleted anisotropically as well, limiting the electron losses to the walls. In such conditions, the plasma can be effectively heated in spite of the emission of cold secondary electrons from the walls, which is frequently considered by fluid theories as an effective mechanism of plasma cooling. In the collisionless regime, energy relaxation of emitted electrons within a thin (compared to the electron mean free path) plasma slab may be caused by the two-stream instability. However, if the velocity distribution of emitted electrons is a monotonically decreasing function, the two-stream instability does not develop,[11] the emitted electrons do not lose energy and freely propagate between the walls of a thruster channel,

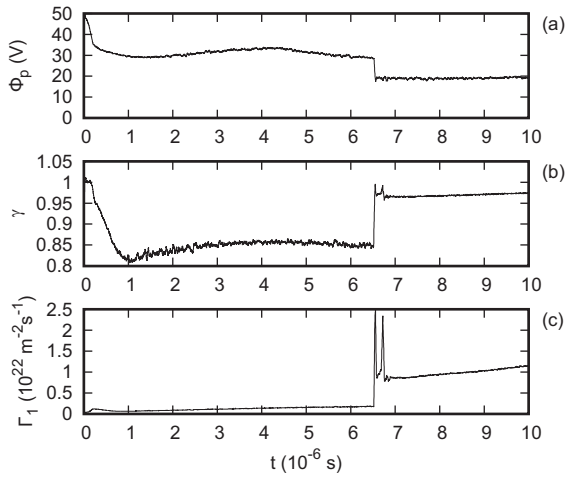

FIG. 2: Temporal evolution of the plasma potential at $x = H/2$ (a), emission coefficient at $x = 0$ (b), and primary electron flux at $x = 0$ (c) in simulation with $E_z = 200$ V/cm, $B_x = 100$ Gauss, $H = 3.3$ cm.

forming counter-streaming secondary electron beams.[12] These beams produce the major part of the electron flux penetrating through the sheath, which results in interesting effects described below.

PIC simulations carried out with intense axial electric field (the detailed description of initial conditions for such simulations is left for Section III) exhibit single sudden changes in numerous plasma parameters during slow temporal evolution, for example as shown in Fig. 2. The jump at $t \approx 6.5 \cdot 10^{-6}$ s in this figure corresponds to the onset of an instability. It is well known that a discharge becomes unstable if one of its regions has a current-voltage characteristic with a negative conductivity (slope).[16] Oscillations related to such instabilities have been studied in vacuum tubes long ago.[17] The instability shown in Fig. 2 is associated with the negative conductivity of the sheath as well.

In general, the sheath is stable if a fluctuation of the plasma potential relative to the wall decays. This potential is closely related to the surface charge on the wall, which is controlled by the balance of ion and electron fluxes towards the wall. Since the ion flux satisfies the Bohm condition and remains essentially unaffected by the fluctuation, the sheath stability must be ensured by the proper electron response. For example, if the potential increases (which means that the wall becomes charged more negatively), the fluctuation will decay and the initial wall charge will be restored if the electron flux to the wall, Γ_e, decreases. This requires the positive conductivity:

$$\frac{\partial J_e}{\partial \Phi_p} > 0 \ , \qquad (1)$$

where $J_e = -e\Gamma_e$ is the electric current towards the wall produced by electrons, $-e$ is the electron charge, and Φ_p is the plasma potential relative to the wall.

Stability condition (1) remains valid in case of a wall with SEE. In this case, the electron response depends also on the properties of the secondary electron flux emitted by the wall. The electron current at the wall with SEE is

$$J_e = -e(\Gamma_1 - \Gamma_2) = -e\Gamma_1(1 - \gamma) \ , \qquad (2)$$

where $\Gamma_{1,2}$ are the primary and the secondary electron fluxes, and $\gamma = \Gamma_2/\Gamma_1$ is the emission coefficient. If for some reason, in the above example the secondary electron flux decreases faster than the primary flux, then the wall will continue to charge negatively and the sheath becomes unstable. The instability of a sheath in the presence of strong SEE has been observed experimentally in Ref. 18, where a 200-eV electron beam was used to strike a wall and produce secondary electron emission. For a Hall thruster, the instability of a single sheath region with a given non-monotonic EVDF of the confined plasma was proposed by Morozov.[19] The sheath instability discussed below appears to be due to the nonlinear dependence of the total electron current in the sheath on the plasma potential relative to the walls. This nonlinear dependence is implemented via a previously unreported mechanism involving (i) oscillation of the energy of secondary electron beams along their trajectory in crossed electric and magnetic fields and (ii) corresponding modification of intensity of SEE produced by these beams themselves.

It is necessary to emphasize that, although the instability was found in simulations, where it appears while the system evolves (converges) towards the final self-consistent stationary state, the instability is not numerical but physical. In a real discharge, the existence of unstable states may result in a jump-like change of discharge parameters in response to a small variation of device dimensions. This agrees qualitatively with the experimental evidence of a strong effect of the plasma channel width on the HT plasma properties[20] and is confirmed by the parametric study in the present paper.

The paper is organized as follows. In Section II, the analytical criterion of the sheath instability is derived and discrete set of stability intervals for the final cyclotron rotation phase of secondary electrons is obtained. Section III describes results of one-dimensional PIC simulations of the acceleration region of a Hall thruster with different values of the gap between the channel walls. The conclusions are given in Section IV. In Appendix A, additional details on the relative importance of competing terms determining the sheath stability criterion are given.

II. RELATION BETWEEN THE SHEATH STABILITY AND THE PHASE OF CYCLOTRON ROTATION OF A SECONDARY ELECTRON

We start with the analysis of modification of the electron current in the sheath in response to a perturbation of the plasma potential. It is necessary to mention that the instability itself (*i.e.*, the jump stage) is a very fast process, which develops on a time scale of the order of the electron flight time between the walls and involves "cross talk" between the sheath regions at the opposite walls. Here, we consider not the jump stage, but the processes preceding the jump, because they explain why the system becomes unstable. For this, we consider plasma potential perturbations that are slow compared to the electron flight time. This allows us to make the quasi-stationary assumption that sheath properties follow a change in the plasma potential in the entire plasma. The perturbation is assumed symmetric so that both sheaths change in the same way. Due to a change in the plasma potential, both the electron flux reaching the wall and the emission coefficient change due to the modification of the electron energy arriving to the wall. Variation of the electron current to the wall is defined by the derivative of Eq. (2) with respect to the plasma potential:

$$\frac{\partial J_e}{\partial \Phi_p} = -e(1-\gamma)\frac{\partial \Gamma_1}{\partial \Phi_p} + e\frac{\partial \gamma}{\partial \Phi_p}\Gamma_1 \ . \tag{3}$$

The influence of the stabilizing first term associated with the decrease of the primary electron flux in case of increased plasma potential $-e\partial\Gamma_1/\partial\Phi_p > 0$ is greatly reduced due to the factor$(1-\gamma)$, which is small because in the regimes of interest the emission coefficient is approaching unity. In this case, the sheath stability condition (1) simplifies:

$$\frac{\partial \gamma}{\partial \Phi_p} > 0 \ . \tag{4}$$

There are two different groups of electrons contributing to the wall flux: (i) the plasma electrons trapped by the ambipolar potential and scattered to the wall by collisions and (ii) the secondary electron beam coming from the opposite wall. Thus, the incoming wall flux is the sum of the flux of collision ejected electrons, Γ_{1p}, and the flux of a secondary electron beam emitted from the opposite wall, Γ_{1b}. Collision-ejected electrons generate a secondary electron flux $\Gamma_{2p} = \gamma_p\Gamma_{1p}$, and the beam electrons generate a secondary electron flux $\Gamma_{2b} = \gamma_b\Gamma_{1b}$, where $\gamma_{p,b}$ are the partial emission coefficients for each electron component. Since in the steady-state of a symmetric system the emitted electrons penetrate through the whole plasma slab and do not thermalize with the plasma electrons,[12] the outgoing secondary electron flux is equal to the flux of the beam of electrons coming from the opposite wall, $\Gamma_{2p} + \Gamma_{2b} = \Gamma_{1b}$. The total emission coefficient is[10]

$$\gamma = \frac{\Gamma_{2p}+\Gamma_{2b}}{\Gamma_{1p}+\Gamma_{1b}} = \frac{\gamma_p}{1+\gamma_p-\gamma_b} \ . \tag{5}$$

For our simulations $\gamma_p \simeq 1.2-1.5$ and $\gamma_b \simeq 0.8-0.95$ yielding γ approaching unity.

Differentiation of (5) with respect to the plasma potential gives

$$\frac{\partial \gamma}{\partial \Phi_p} \sim (1-\gamma_b)\frac{\partial \gamma_p}{\partial \Phi_p} + \gamma_p\frac{\partial \gamma_b}{\partial \Phi_p} \ . \tag{6}$$

Since the velocity distribution of plasma electrons is strongly anisotropic, and the energy (temperature) associated with the direction parallel the walls is much larger than the energy (temperature) associated with the direction normal to the wall, a change in the plasma potential barely modifies the energy of electrons scattered to the walls by collisions. As a result, the partial emission coefficient of collision-ejected electrons γ_p weakly depends on the plasma potential and the variation of γ occurs mostly via the second term in (6). Hence, stability condition (4) can be replaced by

$$\frac{\partial \gamma_b}{\partial \Phi_p} > 0 \ . \tag{7}$$

Relative importance of different terms in Eqs. (3) and (6) is further verified numerically in Appendix A.

Condition (7) links the sheath stability with the variation of the intensity of SEE produced by a secondary electron beam. This value depends on the energy of the beam at the moment of its impact with the wall. Consider a secondary electron emitted from the wall $x = 0$ in the system shown in Fig. 1. The electron (i) is accelerated towards the opposite wall by the x-directed gradient of the electrostatic potential $\Phi(x)$, (ii) performs cyclotron rotation in the $y-z$-plane, and (iii) drifts in the y-direction with the drift velocity $V_{dr} = E_z/B_x$. Let, for simplicity, the initial electron speed be zero (this is a reasonable approximation since most electrons are emitted with the energy much smaller than the energy they acquire during their flight between the walls). After the electron passes through the first sheath region, plasma bulk, and the second sheath region, its energy component along the magnetic field is cancelled. The energy of the electron at the moment of its collision with the wall $x = H$ is due to its motion in the direction perpendicular to the magnetic field and is

$$w_b = mV_{dr}^2\left(1-\cos\varphi_H\right) \ , \tag{8}$$

where $\varphi_H = \omega_c\tau_H$ is the final phase of cyclotron rotation, $\omega_c = eB_x/m$ is the electron cyclotron frequency, $-e$ and m are the electron charge and mass, and

$$\tau_H = \int_0^H dx' \left[\frac{2e\Phi(x')}{m}\right]^{-1/2} \tag{9}$$

is the electron flight time between the walls.

It is reasonable to assume that $\gamma_b = \gamma_b(w_b)$ with $\partial\gamma_b/\partial w_b > 0$. The external parameter that affects the energy w_b is the potential profile $\Phi(x)$ that affects the

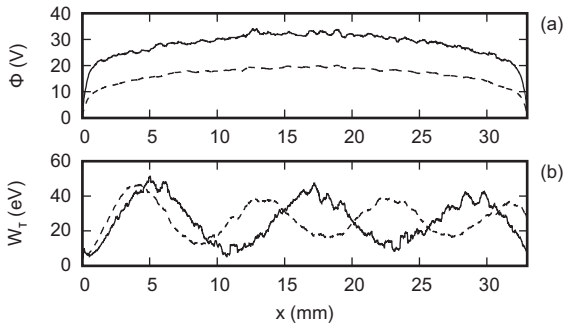

FIG. 3: For simulation shown in Fig. 2, profiles of the potential (a) and the average energy of transverse motion of a secondary electron beam emitted at $x = 0$ at $t = 5.08 \cdot 10^{-6}$ s (solid curves) and $t = 9.991 \cdot 10^{-6}$ s (dashed curves).

electron flight time τ_H. In the considered system the stationary potential profile is symmetric, it has maximum in the midplane $\Phi(H/2) = \Phi_p$ and decays monotonically towards the walls. For simplicity, below we will consider the flight time (9) as a function of the potential profile amplitude Φ_p. Using the chain rule for differentiation in (7) one obtains

$$\frac{\partial \gamma_b}{\partial \Phi_p} = \frac{\partial \gamma_b}{\partial w_b} \frac{\partial w_b}{\partial \tau_H} \frac{\partial \tau_H}{\partial \Phi_p} > 0 \ .$$

Since $\partial \tau_H / \partial \Phi_p < 0$, condition (7) will be satisfied if

$$\frac{\partial w_b}{\partial \tau_H} = m V_{dr}^2 \sin \varphi_H < 0 \ . \qquad (10)$$

From here follows that in the stable state the final cyclotron rotation phase of the secondary electron beam must belong to the following set of intervals:

$$n + \frac{1}{2} < \frac{\varphi_H}{2\pi} < n + 1 \ , \ n = 0, 1, 2, \dots \ . \qquad (11)$$

In (11), the integer number n has the meaning of complete gyro-rotations performed by a secondary electron during its flight between the walls.

The jump shown in Fig. 2 at $t \approx 6.5$ s occurs because the instability develops as the phase crosses the boundary of one of the intervals in (11). Before the jump, the plasma potential amplitude is relatively high (solid curve in Fig. 3a). Define the average transverse energy of a secondary electron beam emitted at $x = 0$ as a function of x-coordinate as $W_T(x) = \langle m[v_y^2(x) + v_z^2(x)]/2 \rangle$, where $v_{y,z}(x)$ are the velocity components, and averaging $\langle ... \rangle$ is performed locally over electrons emitted from the wall $x = 0$. The profile of the average transverse energy depicted by the solid curve in Fig. 3b shows that before the jump a secondary electron performs a little less than 3 rotations during its flight between the walls, which corresponds to $n = 2$ in (11). Slow evolution of the plasma potential preceding the jump is accompanied by a gradual modification of the electron flight time until the phase φ_H increases up to $3 \times 2\pi$, which is the upper boundary for the stability interval with $n = 2$. As soon as the phase reaches this threshold, the sheath becomes unstable with respect to a negative potential perturbation and the plasma potential quickly drops (Fig. 2a) allowing many electrons previously confined by the plasma potential to reach the walls. Due to the EVDF anisotropy, these electrons carry significant energy, which increases the emission coefficient (Fig. 2b) and causes a short-time transition to the space-charge limited (SCL) SEE.[21] The SCL regime is established in order to maintain the balance of ion and electron fluxes at the wall when the emission coefficient exceeds the threshold value γ_{cr}, which is 0.983 for xenon. The transition to the SCL regime is accompanied by very high incident (Fig. 2c) and emitted electron wall fluxes. The SCL regime terminates as soon as the intense fluxes of emitted electrons with relatively low energy (compared to the energy of collision-ejected component of the primary electron flux) reach the opposite walls. Thus, the instability lasts for about the time of electron flight between the walls. After the instability quenches, the plasma potential is lower than before (dashed curve in Fig. 3a), the electron flight time is bigger, and a secondary electron performs about 3.7 rotations (dashed curve in Fig. 3b), which corresponds to the middle of the stability interval (11) with $n = 3$.

In the simulation shown in Figs. 2 and 3, the initial distribution of particles corresponds to a non self-consistent uniform density profile. The slow evolution of the potential triggering the instability takes place while the plasma density evolves towards its final self-consistent profile. In a real thruster, the electron flight time between the walls can be changed by choosing a different channel width H. It is reasonable to expect that small variations of the channel width will result in small variations of the discharge properties. However, at some stage the stability may be reached only for the phase interval (11) with a new n. In this case a small change of H will result in a large modification of discharge properties.

III. NUMERICAL STUDY OF PLASMA PROPERTIES FOR DIFFERENT VALUES OF THE CHANNEL WIDTH

In order to study the influence of channel width H on Hall thruster plasma parameters, a set of simulations was carried out as follows. The constant simulation parameters are the axial electric field $E_z = 200$ V/cm, the magnetic field $B_x = 100$ Gauss, the neutral xenon atom density $N_a = 10^{12}$ cm^{-3}, and the turbulent collision frequency $\nu_t = 7 \cdot 10^5$ s^{-1}. The latter parameter is introduced to account for the anomalous electron mobility across the magnetic field.[22] Initially, the plasma (xenon) has uniform profiles of density $n_0 = 10^{11}$ cm^{-3} and isotropic electron temperature $T_{ex} = T_{ey} = T_{ez} = 10$ eV. The electron component has a drift in the y-direction

with the velocity $V_{dr} = E_z/B_x$. These parameters were chosen to approximate the plasma parameters in the AR of the PPPL Hall thruster[2] operating at voltage 350 V with $H = 2.5$ cm. The width of the plasma channel changes between simulations in the range from 1 cm to 4 cm. Note that the simulation shown in Figs. 2 and (3) belongs to this set and is carried out with $H = 3.3$ cm. In each simulation, the evolution of the system was followed during 10 μs, which was sufficient for attaining a steady state. The steady-state results of the simulations as a function of channel width are presented in Fig. 4.

As it has been shown in Ref. 12, the increase of the plasma gap width H should lead to the increase of the plasma potential Φ_p. When the channel gap is increased, the collision-ejected plasma electron flux to the wall is also increased due to the increase of the volume. The ion flux is determined by the Bohm criterion and remains the same for different H, therefore, to balance the electron and ion fluxes, the plasma potential should increase with H. However, at certain values of H, the plasma potential changes in stepwise manner, see Fig. 4(a) at $H = 1.5$ cm and $H = 3.3$ cm.

The stepwise change of the plasma state occurs because the flight time τ_H changes stepwise in order to maintain the stability criterion (10). Fig. 4(b) shows that the SEE beam cyclotron rotation phase φ_H satisfies (11) with $n = 1$ for 1 cm $\leq H \leq$ 1.2 cm, $n = 2$ for 1.5 cm $\leq H \leq$ 3 cm, and $n = 3$ for 3.3 cm $\leq H \leq$ 4 cm. In fact, the following occurs: variation of H results in gradual modification of the cyclotron rotation phase φ_H until it belongs to the stability interval (11) with a constant number of complete rotations n. When the value of H becomes such that the phase cannot stay within the boundaries of (11) for the old n, the plasma transits to the stable state with another n. In other words, the number of complete rotations performed by secondary electrons during their flight between the walls changes. To illustrate this point, the profiles of the average z-directed velocity of SEE beams obtained in the simulations shown in Fig. 4 are plotted in Fig. 5. In this figure, panel (a) shows that the secondary electrons perform about $1\frac{3}{4}$ rotations, panel (b) shows $2\frac{3}{4}$ rotations, and panel (c) shows $3\frac{3}{4}$ rotations.

According to the phase condition (11), two neighboring stable states with close H but different numbers of complete rotations, n and $n+1$, have a difference in the SEE beam cyclotron rotation phase of about π. This explains why the SEE beam energy (8) is noticeably different in such states, as one can see in Fig. 4(c). Correspondingly, the emission coefficient γ [Fig. 4(d)] and the primary electron flux to the wall Γ_1 change abruptly. Since Γ_1 depends on the plasma density, which is different in every simulation and may obscure the phase-related effect, in Fig. 4(e) we present the effective frequency of electron scattering by the walls defined as $\nu_w = 2\Gamma_1/\langle n_e\rangle H$, where $\langle n_e\rangle$ is the plasma density averaged over the plasma gap. This frequency defines the electron mobility across the magnetic field due to the near-wall conductivity effect.[23,24] Our simulations show that variation of the SEE beam energy in response to the modification of H can produce values of ν_w much higher than both the selected turbulent collision frequency ν_t [dash-dot line in Fig. 4(e)] and the frequency of electron collisions with neutral atoms ν_{en} [diagonal crosses in Fig. 4(e)]. In this case the near-wall conductivity

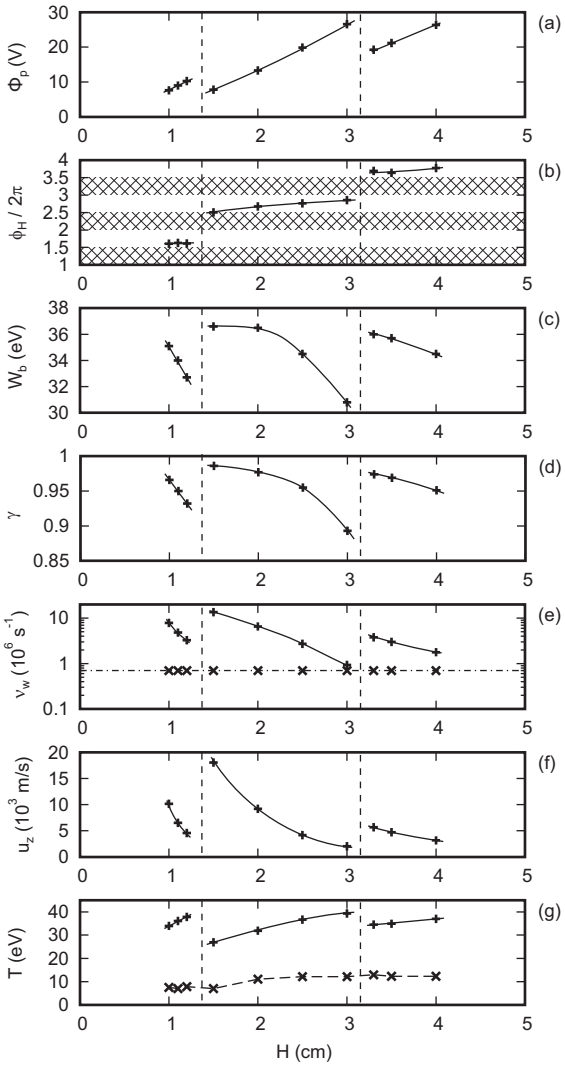

FIG. 4: Dependence of discharge parameters on the width of the plasma gap. (a) Plasma potential in the midplane. (b) SEE beam cyclotron rotation phase, cross-hatched areas mark unstable states. (c) SEE beam energy at the moment of impact with the target wall. (d) Total emission coefficient. (e) Effective frequency of electron scattering by the walls of the plasma channel (solid line with straight crosses), frequency of electron-neutral collisions (diagonal crosses), and frequency of turbulent collisions (dash-dot line). (f) Electron flow velocity in the z-direction. (g) Electron temperature in the z-direction (solid line with straight crosses) and in the x-direction (dashed line with diagonal crosses). Markers (crosses) mark the values obtained in simulations, curves are the result of interpolation.

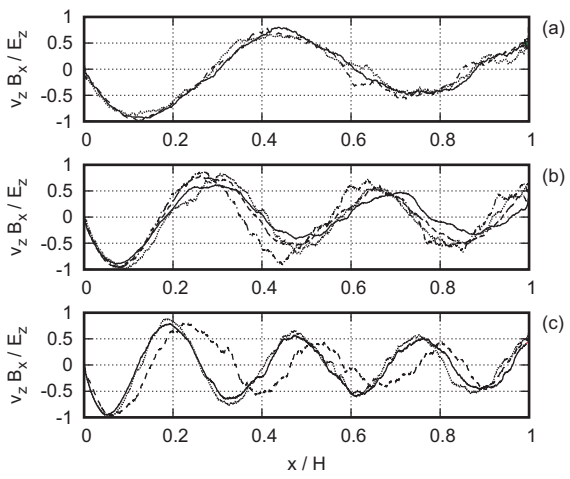

FIG. 5: Profiles of the z-directed flow velocity of the secondary electron beam emitted from the wall $x = 0$. (a) Simulations with $H = 1$ cm (solid curve), 1.1 cm (dash curve), and 1.2 cm (dot curve). (b) Simulations with $H = 1.5$ cm (solid), 2 cm (dash), 2.5 cm (dot), and 3 cm (dash-dot). (c) Simulations with $H = 3.3$ cm (solid), 3.5 cm (dash), and 4 cm (dot).

becomes the dominant mechanism of electron transport along the axis of a Hall thruster. The non-monotonic behavior of ν_w results in the non-monotonic dependence of the axial electron flow velocity u_z shown in Fig. 4(f).

The electron temperature along the z-direction, T_{ez}, shown in Fig. 4(g) repeats qualitatively the shape of the dependence $\Phi_m(H)$ in Fig. 4(a). This agrees with the idea that the plasma potential in HT depends on T_{ez} and on scattering of plasma electrons to the loss cone.[12] The electron temperature normal to the walls T_{ex} changes less noticeably [dashed curve in Fig. 4(g)].

IV. CONCLUDING REMARKS

Summarizing, in many plasmas, the potential profile in the stable steady-state corresponds to the positive conductivity of the current-voltage characteristic. When applied to a sheath near a wall emitting secondary electrons, for example in the channel of a Hall thruster, this imposes a condition that the total electron current to the wall $J_e = -e(\Gamma_1 - \Gamma_2)$ should increase as the plasma potential relative to the wall increases, $\partial J_e/\partial\Phi_p > 0$. In the opposite case, an instability develops if the conductivity of the current-voltage characteristic of the sheath is negative, $\partial J_e/\partial\Phi_p < 0$.

When SEE is strong, the contribution of secondary electrons emitted at one wall to the primary electron flux to the opposite wall may be dominant. In this case, the sheath conductivity may become negative and the plasma potential, correspondingly, unstable due to a strong dependence of the beam energy on the plasma potential implemented via the time of electron flight between the walls. This instability has been observed in a numerical study of the dependence of plasma parameters in the acceleration region of a Hall thruster on the width of the plasma channel carried out with a 1D3V PIC code. We found that at certain values of the channel width, when the final phase of cyclotron rotation of a secondary electron beam belongs to an interval $[2\pi k,\ 2\pi(k + 1/2)]$ with k integer, the plasma potential becomes unstable and changes so that the phase belongs to a new interval $[2\pi(n + 1/2),\ 2\pi(n + 1)]$ with n integer. In our simulations, $k = n$, however, this is not necessary.

As a result, numerous plasma parameters in the steady state may change in a stepwise manner. In particular, the effective frequency of electron-wall scattering becomes a non-monotonic function of the channel width. This frequency defines the contribution of the near-wall conductivity effect to the electron current and for some values of the channel width this contribution may significantly exceed the axial electron transport due to other mechanisms, such as turbulence or electron scattering on neutral atoms.

The developed theory is applicable when the electric field in the channel is so large that the secondary electron emission is intense ($\gamma \to 1$). This corresponds to a large azimuthal drift velocity, so that the corresponding energy of drift motion acquired by an electron emitted from one wall is enough to produce SEE upon its impact with the opposite wall. Such a regime occurs when the axial electric field is large ($E_z > 200$ V/cm) and is typical for Hall thrusters operating under high voltages (above 400 V).[20] In the low-voltage regime, when the axial electric field is small ($E_z < 100$ V/cm) and the azimuthal drift of secondary electron beams is slow, the effect of the cyclotron rotation phase on the system properties is much weaker.

This research was partially supported by the Air Force Office of Scientific Research through the AF STTR Program and the U. S. Department of Energy Office of Fusion Energy Sciences. Simulations were carried out using the WestGrid facilities in the University of British Columbia.

APPENDIX A: RELATIVE IMPORTANCE OF COMPETING TERMS IN THE ELECTRON CURRENT AND EMISSION COEFFICIENT DERIVATIVES

Equation (3) can be written in the form

$$\frac{\partial J_e}{\partial \Phi_p} = a_\Gamma + a_\gamma \ ,$$

where

$$a_\Gamma \equiv e\frac{\partial \Gamma_1}{\partial \Phi_p}(\gamma - 1), \quad a_\gamma \equiv e\Gamma_1\frac{\partial \gamma}{\partial \Phi_p} \ .$$

Equation (6) can be written in the form

$$\frac{\partial\gamma}{\partial\Phi_p} \sim a_p + a_b \ ,$$

where

$$a_p \equiv (1-\gamma_b)\frac{\partial\gamma_p}{\partial\Phi_p}, \quad a_b \equiv \gamma_p\frac{\partial\gamma_b}{\partial\Phi_p} \ .$$

The criterion of stability (10) and the set of intervals (11) are obtained assuming that

$$a_\Gamma \ll a_\gamma, \quad a_p \ll a_b \ . \tag{A1}$$

In general, this requires both the intense SEE ($\gamma \approx 1$) and high electron azimuthal drift energy ($\gamma_b \approx 1$). It is instructive to check inequalities (A1) directly, using the electron data and potential profiles obtained in the PIC simulations. The value of γ, for example, can be calculated using the EVDF in the midplane $f(\mathbf{v}, H/2)$ obtained self-consistently in simulation:

$$\gamma = \frac{\int_{v_*}^{\infty} dv_x v_x \int_{-\infty}^{\infty} dv_y \int_{-\infty}^{\infty} dv_z f(\mathbf{v}, H/2)\gamma(H)}{\int_{v_*}^{\infty} dv_x v_x \int_{-\infty}^{\infty} dv_y \int_{-\infty}^{\infty} dv_z f(\mathbf{v}, H/2)} \ ,$$

where $v_*^2 = 2e\Phi_p/m$, $\gamma(H) \equiv \gamma\left[w_x(H), w_t(H)\right]$ is the emission coefficient, $w_x(H) = mv_x^2/2 - e\Phi_p$ is the energy of electron motion in the direction normal to the wall at the moment of impact with the wall $x = H$, and $w_t(H) = m(v_y^2 + v_z^2)/2$ is the energy of electron motion parallel to the walls at the moment of impact with the wall. The latter energy is a function of the phase of cyclotron rotation in crossed fields E_z and B_x:

$$w_t(H) = \frac{m(v_y^2+v_z^2)}{2} + mV_{dr}^2\left[\left(1-\frac{v_y}{V_{dr}}\right)\left(1-\cos\omega_c\tau_{H/2}\right) - \frac{v_z}{V_{dr}}\sin\omega_c\tau_{H/2}\right] \ ,$$

where $\tau_{H/2}$ is the duration of the electron flight from the midplane $x = H/2$ to the wall $x = H$, calculated as

$$\tau_{H/2} = \int_{H/2}^{H} dx\left[v_x^2 + \frac{2e\Phi(x)}{m}\right]^{-1/2} \ , \tag{A2}$$

where v_x, v_y and v_z are the velocity components of an electron in the midplane $x = H/2$.

To calculate γ as a function of the potential in the midplane Φ_p, one can represent the potential profile in (A2) as $\Phi(x) \approx \Phi_p \times \psi(x)$, where the shape function $\psi(x)$ remains unchanged. The shape function was interpolated as

$$\psi(x) = (1 - |2x/H - 1|^k)^{1/k},$$

where $2 < k < 3$. It is important that for different values of Φ_p one still has to use the same EVDF $f(\mathbf{v}, H/2)$ obtained self-consistently in simulation. This procedure is partially non-self-consistent, which is why the dependence $\gamma(\Phi_p)$ obtained as above is meaningful only in close proximity to the actual values of γ and Φ_p. The dependencies $\Gamma_1(\Phi_p)$, $\gamma_p(\Phi_p)$, and $\gamma_b(\Phi_p)$ can be calculated similarly. With these functions available, calculation of coefficients $a_{\Gamma,\gamma,p,b}$ becomes straightforward.

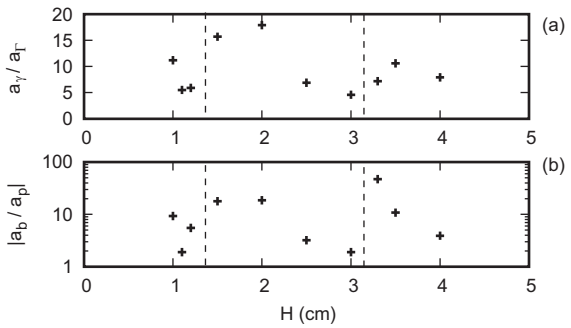

FIG. 6: Ratios of coefficients a_γ/a_Γ (a) and a_b/a_p (b) for simulations with different plasma gap described in Fig. 4.

The ratios of terms a_γ/a_Γ and a_b/a_p for all simulations included in Fig. 4 are presented in Fig. 6(a) and Fig. 6(b), respectively. The first ratio never becomes less than five, while the second ratio never drops below two (and is above four for most cases). Therefore, the theory described in Section II is indeed applicable to the simulations carried out.

* At present time D. Sydorenko is at the University of Alberta, Edmonton T6G 2G7, Canada.

[1] V. V. Zhurin, H. R. Kaufman, and R. S. Robinson, Plasma Sources Sci. Technol. **8**, R1 (1999).

[2] Y. Raitses, D. Staack, A. Smirnov, and N. J. Fisch, Phys. Plasmas **12**, 073507 (2005).

[3] I. D. Kaganovich and L. D. Tsendin, IEEE Trans. Plasma Sci. **20**, 66 (1992).

[4] M. Hirakawa and Y. Arakawa, in *Proceedings of the 24th International Electric Propulsion Conference, Moscow, Russia, September 1995* (Electric Rocket Propulsion Society, Cleveland, OH, 1995), IEPC Paper No. 95-164.

[5] N. B. Meezan and M. A. Cappelli, Phys. Rev. E **66**, 036401 (2002).

[6] J. C. Adam, A. Heron, and G. Laval, Phys. Plasmas **11**, 295 (2004).

[7] F. Taccogna, S. Longo, and M. Capitelli, Phys. Plasmas **12**, 093506 (2005).

[8] F. Taccogna, S. Longo, M. Capitelli, and R. Schneider, in *Proceedings of the 30th International Electric Propulsion Conference, Florence, Italy, September 2007* (Electric Rocket Propulsion Society, Cleveland, OH, 2007), IEPC

Paper No. 2007-12.
[9] D. Sydorenko, A. Smolyakov, I. Kaganovich, and Y. Raitses, IEEE Trans. Plasma Sci. **34**, 815 (2006).
[10] D. Sydorenko, A. Smolyakov, I. Kaganovich, and Y. Raitses, Phys. Plasmas **13**, 014501 (2006).
[11] D. Sydorenko, A. Smolyakov, I. Kaganovich, and Y. Raitses, Phys. Plasmas **14**, 013508 (2007).
[12] I. Kaganovich, Y. Raitses, D. Sydorenko, and A. Smolyakov, Phys. Plasmas **14**, 057104 (2007).
[13] D. P. Schmidt, N. B. Meezan, W. A. Hargus Jr., and M. A. Cappelli, Plasma Sources Sci. Technol. **9**, 68 (2000).
[14] B. Pote, V. Hruby, and R. Tedrake, in *36th AIAA/ASME/SAE/ASEE Joint Propulsion Conf. and Exhibit, Huntsville, AL, July 2000* (American Institute of Aeronautics and Astronautics, Reston, VA, 2000), AIAA Paper No. 2000-3249.
[15] D. Sydorenko, Ph.D. thesis, University of Saskatchewan (2006), http://library2.usask.ca/theses/available/etd-06142006-111353.
[16] Y. P. Raizer, *The Physics of Gas Discharge* (Nauka, Moscow, 1992).
[17] A. W. Hull, Proc. Inst. Radio Electron. Eng. Aust. **6**, 5 (1918).
[18] R. L. Stenzel, Phys. Rev. Lett. **60**, 704 (1988).
[19] A. I. Morozov, Sov. J. Plasma Phys. **17**, 393 (1991).
[20] Y. Raitses, D. Staack, M. Keidar, and N. J. Fisch, Phys. Plasmas **12**, 057104 (2005).
[21] G. D. Hobbs and J. A. Wesson, Plasma Phys. **9**, 85 (1967).
[22] A. Smirnov, Y. Raitses, and N. Fisch, Phys. Plasmas **11**, 4922 (2004).
[23] A. I. Morozov, Zh. Prikl. Mekh. Tekh. Fiz. **3**, 19 (1968), Journal of Applied Mechanics and Technical Physics, in Russian.
[24] M. Keidar and I. I. Beilis, IEEE Trans. Plasma Sci. **34**, 804 (2006).

The Princeton Plasma Physics Laboratory is operated
by Princeton University under contract
with the U.S. Department of Energy.

Information Services
Princeton Plasma Physics Laboratory
P.O. Box 451
Princeton, NJ 08543

Phone: 609-243-2750
Fax: 609-243-2751
e-mail: pppl_info@pppl.gov
Internet Address: http://www.pppl.gov